Localization versus inhomogeneous superfluidity: Submonolayer ^{4}He on fluorographene, hexagonal boron nitride, and graphene

Saverio Moroni
CNR-IOM Democritos and SISSA, Via Bonomea 265, 34136 Trieste, Italy

Francesco Ancilotto and Pier Luigi Silvestrelli
*Dipartimento di Fisica e Astronomia 'Galileo Galilei' and CNISM, Università di Padova, via Marzolo 8, 35122 Padova, Italy
and CNR-IOM Democritos, Via Bonomea 265, 34136 Trieste, Italy*

Luciano Reatto
Dipartimento di Fisica, Università degli Studi di Milano,via Celoria 16, 20133 Milano, Italy

We study a submonolayer ^{4}He adsorbed on fluorographene (GF) and on hexagonal boron nitride (hBN) at low coverage. The adsorption potentials have been computed *ab initio* with a suitable density functional theory including dispersion forces. The properties of the adsorbed ^{4}He atoms have been computed at finite temperature with path integral Monte Carlo and at $T = 0$ K with variational path integral. From both methods we find that the lowest energy state of ^{4}He on GF is a superfluid. Due to the very large corrugation of the adsorption potential this superfluid has a very strong spatial anisotropy, the ratio between the largest and smallest areal density being about 6, the superfluid fraction at the lowest T is about 55%, and the temperature of the transition to the normal state is in the range 0.5–1 K. Thus, GF offers a platform for studying the properties of a strongly interacting highly anisotropic bosonic superfluid. At a larger coverage ^{4}He has a transition to an ordered commensurate state with occupation of 1/6 of the adsorption sites. This phase is stable up to a transition temperature located between 0.5 and 1 K. The system has a triangular order similar to that of ^{4}He on graphite but each ^{4}He atom is not confined to a single adsorption site and the atom visits also the nearest neighboring sites giving rise to a novel three-lobed density distribution. The lowest energy state of ^{4}He on hBN is an ordered commensurate state with occupation of 1/3 of the adsorption sites and triangular symmetry. A disordered state is present at lower coverage as a metastable state. In the presence of an electric field the corrugation of the adsorption potential is slightly increased but up to a magnitude of 1 V/Å the effect is small and does not change the stability of the phases of ^{4}He on GF and hBN. We have verified that also in the case of graphene such electric field does not modify the stability of the commensurate $\sqrt{3} \times \sqrt{3}R30°$ phase.

I. INTRODUCTION

Bosons moving in a periodic external potential $V_{ext}(\mathbf{r})$ can be found in two different states: Depending on the amplitude of the modulation of the external potential either the bosons are localized at the minima of $V_{ext}(\mathbf{r})$ or the bosons are delocalized and superfluid at low temperature. For very strong interboson interaction an incommensurate solid can be present. These two regimes, localized or delocalized, have been achieved with cold bosonic atoms moving in the periodic potential generated by optical standing waves [1]. Also a submonolayer film of light bosons like ^{4}He atoms adsorbed on a crystalline substrate is expected to show one of these two regimes depending on the character of the adsorption potential. In practice so far the only substrate that can approach such an ideal situation is graphite because this material can be obtained with an extended almost perfect surface on which one can study the properties of the adsorbed species [2]. It turns out that the He-graphite adsorption potential is characterized

by a corrugation that is large enough so that the He atoms are localized around the preferential adsorption sites and in fact experiment [2] and theory [3,4] agree that the ground state of a monolayer ^{4}He is an ordered commensurate state in which the ^{4}He atoms occupy one third of the adsorption sites so the adatoms have a crystalline triangular symmetry, the so-called $\sqrt{3} \times \sqrt{3}R30°$ phase. Therefore ^{4}He on graphite is nonsuperfluid, superfluidity appearing only when at least two layers are present [5,6].

On theoretical basis a similar behavior is expected for the adsorption of ^{4}He on graphene (G) because its adsorption potential turns out to be very similar to that of graphite. Other substrates commonly used in adsorption studies are intrinsically disordered like that of a glass or are in any case too disordered to be relevant on this issue. It would be of great interest to find other materials with extended crystalline surfaces with a corrugation of the adsorption potential smaller than that of graphite because this would give the possibility of a new superfluid state of strongly interacting particles that

will be spatially anisotropic due to the influence of the substrate potential. It has been of interest that recent theoretical studies [7,8] found that for two derivatives of graphene, fluorographene (GF), and graphane (GH), the adsorption potential is very different from that of graphene and of graphite and it turns out that the ^{4}He atoms are delocalized and the ground state of monolayer ^{4}He on GF and on GH was claimed to be superfluid. That study was based on a semiempirical adsorption potential. These results have been corroborated by a more recent study [9] in which some of us have developed an adsorption potential based on *ab initio* methods: Even with such adsorption potential it was found that the ^{4}He atoms on GF are delocalized and the ground state of submonolayer ^{4}He is a superfluid. Interestingly, that work [9] has shown that also the monolayer of ^{4}He on hexagonal boron nitride (hBN) turned out to be a superfluid.

Studies of Refs. [7–9] are based on state of the art many body computations that should be able to provide exact results for the system. However quantum simulations of particles in a highly structured potential can be tricky due to the multiple energy scales that are present, and we decided to perform a new investigation of the adsorption of ^{4}He atoms on GF, hBN, and G. In the present study, we have also derived the adsorption potential in the presence of an external electric potential that is a possible way to alter the corrugation of the adsorption potential.

We have studied ^{4}He on GF and hBN at $T = 0$ K with the variational path integral (VPI) method [10], also known as path integral ground state (PIGS) [11], and at finite temperature with path integral Monte Carlo (PIMC) method [10]. In a VPI computation the quantum state is obtained by projecting an assumed initial state with the imaginary time evolution operator. For large enough propagation time β one gets an unbiased sampling [12] of the properties of the exact ground state of the system if the initial state is not orthogonal to the ground state. How large β has to be must be found empirically in terms of convergence. Our evidence is that the results in Refs. [7–9] were not fully converged. We are confident that the present VPI results are at convergence also because they are in agreement, as expected, with those of PIMC at low temperature.

In the case of ^{4}He on GF we confirm the main result of the previous studies [7,9]: The ground state of ^{4}He on GF is a superfluid that has a strong spatial modulation. At variance with the result of Refs. [7,9], we find that at coverage larger than that of the equilibrium state there is a first order phase transition to a commensurate state with triangular symmetry at a coverage corresponding to the occupation of 1/6 of the adsorption sites.

On the other hand, in the case of ^{4}He on hBN, we do not confirm the previous result of the existence of a superfluid state and our results show that, in the ground state and at low temperature, ^{4}He atoms on hBN form a nonsuperfluid commensurate state very similar to that of ^{4}He on graphite. For all the considered substrates we also find that the change of the adsorption potential due to the application of an external electric field E is not large enough to alter in a significant way the properties for $E = 0$, at least for the strength of E allowed by our approximations (see below).

The contents of the paper are as follows. In Sec. II we present the results for the adsorption potential of He on GF, hBN, and G with and without an external electric field. The quantum simulations of our study are described in Sec. III. A summary and our conclusion are contained in Sec. IV. Technical details of the quantum simulations are given in the Appendix.

II. POTENTIALS

Monolayer ^{4}He films on GF and GH have been proposed recently as novel superfluid systems characterized by strong in-plane anisotropies. This remarkable prediction [7,8,13,14] was based on quantum simulations where an essential ingredient is an accurate description of the interaction between He atom and the substrates. Specifically, the He-substrate interaction potential was modeled using a traditional semiempirical approach [15], where the potential energy of a single He atom near the surface is written as a sum of pair potential interactions made of a repulsive part proportional to the local electron density (Hartree-Fock repulsion), and an attractive part, in the form of a sum of damped He atom van der Waals (VdW) interactions and polarization interaction due to the surface electric field [7,13,14].

These effective potentials are known to be affected by quite large uncertainties in the empirical coefficients used to model the interaction. The importance of a precise knowledge of the adatom-surface interaction potentials to make quantitative prediction on the adsorption properties of surfaces cannot be overlooked: The wetting properties of rare-gas atoms on solid surfaces, for instance, are known to strongly depend on the strength and corrugation of the adatom-substrate potential.

For this reason, we decided to investigate from first principles the interaction of He atoms with GF and hBN using state-of-the-art density functional theory (DFT) functionals specifically designed to describe the weak VdW interactions, with the goal of providing a more accurate description of the interaction of He atoms with these surfaces. Recent applications of vdW-corrected DFT schemes to the problem of atoms/molecules-surface interactions have proven the accuracy of such methods in the calculation of both adsorption distances and adsorption energies, as well as the high degree of its reliability across a wide range of adsorbates. In particular, we have computed the He atom adsorption energies on different surface sites and the potential energy corrugations along the plane, which are the most crucial ingredients for accurate quantum simulations of the adsorption of ^{4}He. Our calculations have been performed with the QUANTUM-ESPRESSO *ab initio* package [16]. A single He atom per supercell is considered, and we model the substrates adopting periodically repeated orthorhombic supercells, with a 4×2 structure, in the case of G with 64 C atoms, in the case of GF with 32 C atoms plus as many F atoms, while in the case of hBN the substrate is formed by 16 B and 16 N atoms. The lattice constants correspond to the equilibrium state of the substrates. Repeated slabs were separated along the direction orthogonal to the surface by a vacuum region of about 24 Å to avoid significant spurious interactions due to periodic replicas. The Brillouin zone has been sampled using a $2 \times 2 \times 1$ k-point mesh. Electron-ion interactions were described using

TABLE I. Best-fit parameters for the z dependence of the He-substrate potentials shown in Fig. 2.

		a_1	b_1	a_2	b_2	c_1	c_2	c_3	c_4
GF:	TF	2.53645×10^7	1.55209	1.07222×10^6	0.842514	-4.49616×10^6	7.37512×10^8	-5.63025×10^9	1.19823×10^{10}
	B	-4.25772×10^8	2.63907	-1.0177×10^7	1.61871	-339981	7.38605×10^7	-3.58557×10^9	1.1976×10^{10}
	H	-2.73175×10^6	1.91148	-2.77692×10^6	1.91101	42978.4	8.18279×10^6	-3.9442×10^8	1.54338×10^9
	TC	526386	0.975559	20543.4	0.389085	4.68048×10^6	8.32948×10^6	-4.34654×10^8	1.61137×10^9
hBN:	TN	-244960	1.94545	-231170	1.94594	93994	-1.97338×10^6	1.6644×10^6	2.86811×10^6
	B	2.15693×10^7	3.62009	2.03143×10^7	3.61956	87334	-2.0872×10^6	2.18302×10^7	-3.33307×10^7
	TB	-208875	1.90869	-218649	1.90819	99505.8	-2.25015×10^6	4.40446×10^6	-1.32199×10^6
	H	1.75506×10^7	3.56209	1.7902×10^7	3.56201	89581.7	-2.20804×10^6	2.3581×10^7	-3.80861×10^7

ultrasoft pseudopotentials and the wave functions were expanded in a plane-wave basis set with an energy cutoff of 51 Ry.

The calculations have been performed by adopting the rVV10 [17] DFT functional (this is the revised, more efficient version of the original VV10 scheme [18]), where vdW effects are included by introducing an explicitly nonlocal correlation functional. rVV10 has been found to perform well in many systems and processes where vdW effects are relevant, including several adsorption processes [17,19,20]. This DFT functional is able to well reproduce the reference structural data of GF, hBN, and G including the "buckling displacement" in GF [7,13,14].

We have also investigated the effect of the application of an external uniform electric field. Since in supercell calculations periodic boundary conditions are imposed on the electrostatic potential, an external electric field is simulated by adding a sawlike potential to the bare ionic potential [21], also including a dipole correction, according to the recipe of Bengtsson [22]. This represents the proper way to simulate an external electric field in surface calculations with a slab geometry, provided the electrostatic potential discontinuity falls in the middle of the vacuum region [21–23]. A positive value means that the external electric field points away from the surface in the positive z direction (the adsorbed He atom is located in the positive z region). The additional external potential also leads to changes in the total energy of the system and the Hellmann-Feynman forces [23].

An upper limit for the amplitude of the external electric field, which can be considered in the simulations, exists that is determined by the thickness of the vacuum region. In fact a kind of "quantum well" is formed in the vacuum region [23]; if the electrostatic potential of this quantum well drops below the Fermi level, it can become populated by the transfer of electrons from the slab region: The threshold for the occurrence of this unwanted, artificial behavior depends on both the width of the vacuum region and the strength of the electric field [23]. In our applications this upper limit turns out to be around 1.0 V/Å, which is a value of the same order (or even larger) than the maximum electric field achievable in actual experiments (for instance, in electrowetting applications [24]).

We computed the He-substrate interaction (with and without electric field) for a selected set of nonequivalent sites in the primitive surface unit cell. In particular, for He on GF, we chose the following points: H (hollow site), TC (site on top of C atom), TF (site on top of F atom), B (bridge site between C and F); for He on hBN we chose: H (hollow site), TB (site

on top of B atom), TN (site on top of N atom), B (bridge site between B and N); finally, for He on G, we considered the points: H (hollow site), TC (site on top of C atom), and B (bridge site between two adjacent C atoms). The sites for GF and hBN are shown in Fig. 1.

Besides the lowest-energy configurations for a given investigated adsorption site, we have also computed the dependence upon the normal coordinate z of the He-substrate interaction potentials above those sites, shown in Fig. 2. Our goal was to provide a reliable three-dimensional He-substrate potential function to be used for numerical simulations based on quantum Monte Carlo methods that will be discussed in the following.

We approximate such potential by using a truncated Fourier expansion over the first three stars of the two-dimensional reciprocal lattice associated with a triangular lattice with a two-atom basis (two C atoms in the case of G, one C and one F atom in the case of GF, one B and one N atom in the case of hBN). The Fourier components can be obtained from the calculated z dependence of the various symmetry sites described above [25].

Our numerical results for the adsorption of He on the different substrates we have considered are summarized in Table II. In particular, we report the distance d of He from the substrate and the binding energy E_b of the the lowest-energy configuration. This configuration is found above the hollow site H for hBN and G and above the TC site for
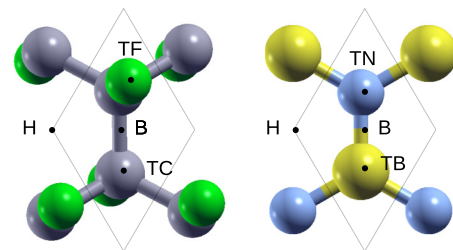

FIG. 1. Sites chosen for the calculation of the He-GF (left panel) and He-hBN (right panel) potentials. GF has a three-layer structure: The central layer is occupied by the carbon atoms as in a graphene sheet except for a small vertical offset between the two triangular sublattices, the upper plane, and the lower one contain the fluorine atoms. In the left panel C atoms are shown as gray circles and F atoms as green circles. hBN is a single layer structure isomorphous to graphene. In the right panel B atoms are shown as yellow circles and N atoms as blue circles.
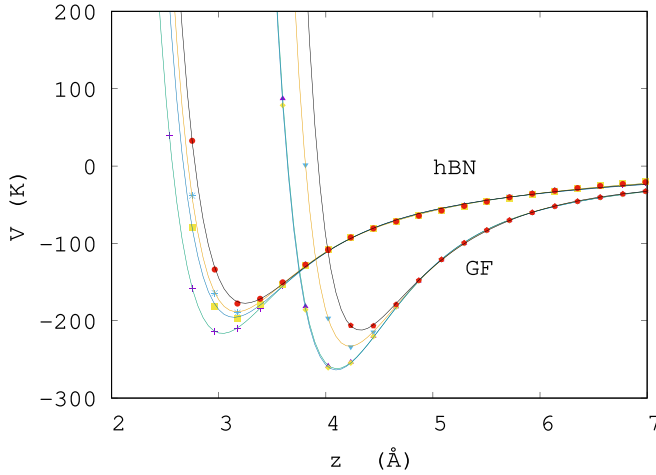
FIG. 2. Calculated He-hBN and He-GF interaction potentials along the z direction above selected sites. GF (from top to bottom): TF, B, H, TC; hBN (from top to bottom): TN, B, TB, H. The points show the *ab initio* values; the lines are the results of eight-parameter curve fitting with the form $\sum_{i=1}^{2} a_i \exp(-b_i z) - \sum_{i=1}^{4} c_i/z^{2i+2}$, whose parameters are given in Table I.

GF (see Fig. 2). For GF a nearly isoenergetic configuration is found also above the hollow site [7,9]. Therefore on GF two essentially equivalent kinds of adsorption sites are present and the overall number of adsorption sites is double that on hBN and G. In Table II we also report two other energetic parameters: the "maximum corrugation" Δ_{max}, defined as the difference between the binding energy of He on top of C, F, and N atoms (which represents the less-favored configuration for G, GF, and hBN, respectively) and the binding energy of the lowest-energy configuration, and the "minimum intersite energy barrier" Δ_{min}, which is given by the minimum energy barrier that the He atom must overcome to be displaced from an optimal adsorption site to another, namely from H to H for hBN and G and from H to TC for GF. This latter quantity has been evaluated by monitoring the binding energy corresponding to a reaction path generated by constraining the planar x, y coordinates of the He atom and optimizing the vertical z coordinate only. In the case of hBN, Δ_{min} (Δ_{max}) corresponds to the difference between the binding energy of He on top of

TABLE II. Binding energy in the lowest-energy configuration (with and without external electric field) E_b, distance d of He from the reference plane (defined by averaging over the z coordinates of the C atoms for G and GF, and of the B and N atoms for hBN), maximum corrugation Δ_{max}, minimum intersite energy barrier Δ_{min} (see text for the definitions), for He-G, He-GF, and for He-hBN, using the rVV10 DFT functional.

System	Electric field (V/Å)	E_b (K)	d (Å)	Δ_{max} (K)	Δ_{min} (K)
He-GF	0.0	−261	4.10	54	11
He-GF	1.0	−278	4.10	55	10
He-hBN	0.0	−214	2.96	36	16
He-hBN	1.0	−235	2.96	43	19
He-G	0.0	−298	2.96	50	47
He-G	0.6	−290	2.96	47	44

the B (N) atom, $TB(TN)$ site, and the binding energy of the lowest-energy configuration H.

For the case of no external electric field, the results for the corrugation of the adsorption potential agree with those reported in previous studies [7,9,26]: The most striking difference between the case of He-G and of He-GF is that in He-G Δ_{max} and Δ_{min} are comparable (the difference is about 7%) while, on the contrary, in He-GF Δ_{min} is smaller than Δ_{max} by a factor 5. This confirms that the adsorption potential of He on GF is characterized by narrow "canyons" between adsorption sites, with a much larger anisotropy in the corrugation and a relatively low energy barrier compared to G. A large difference between Δ_{min} and Δ_{max} (about a factor 2) is found also for hBN so that the corrugation is larger than in the case of G. Another difference between hBN and G is that each adsorption site in hBN is surrounded by three saddle points and not six as in the case of G and graphite. It should be noticed that the adsorption energy of He on GF found with the semiempirical approach in Ref. [7] appears to be strongly overestimated, we find that this energy is about 10% smaller than that on G and not much larger as reported in Ref. [7].

When an external, uniform electric field is applied (with the maximum strength of E allowed by our approximations, see discussion above), there is a change of the adsorption potential, leading to moderate quantitative changes in the quantities reported in Table II, which, however, are not so significant to alter the basic properties found at vanishing electric field.

III. QUANTUM SIMULATIONS

We use the rVV10 potentials of Sec. II to calculate unbiased equilibrium thermal averages and ground-state properties of ^{4}He adsorbed on GF, hBN, and G with quantum Monte Carlo simulations. For N He atoms the Hamiltonian is

$$H = -\frac{\hbar^2}{2m}\nabla^2 + \sum_{i=1}^{N} + v_1(\mathbf{r}_i) + \sum_{i<j} v_2(r_{ij}), \quad (1)$$

where v_1 is the appropriate He-substrate one-body potential with $\mathbf{r}_i$ the position of the ith ^{4}He atom, and v_2 is the Aziz HFDHE2 He-He pair potential [27] with $r_{ij} = |\mathbf{r}_i - \mathbf{r}_j|$. The substrate is placed at $z = 0$ with the ^{4}He atoms in the positive z semispace, and periodic boundary conditions are applied in the x and y directions.

The finite temperature simulations are performed using the PIMC method [10] with the worm algorithm [28]. In this approach the matrix element $\langle R|e^{-\beta H}|PR\rangle$, where β is the inverse temperature, $R = \{\mathbf{r}_1, \ldots, \mathbf{r}_N\}$, and PR is a permutation thereof, is represented as a real-space convolution of M high-temperature density matrices $\langle R'|e^{-\tau H}|R''\rangle$, where $\tau = \beta/M$, which are in turn approximated by suitable closed-form expressions. The results are unbiased in the limit $\tau \to 0$. We use the primitive approximation [10] with $\tau = 0.002$ K^{-1}. In the Appendix we show that the finite-τ systematic error is negligible for our purposes. We work in the grand canonical ensemble, i.e., at fixed volume V, temperature T, and chemical potential μ.

The ground state simulations are performed with a projection Monte Carlo method known as VPI [10] or PIGS [11]. This approach uses the same real-space convolution
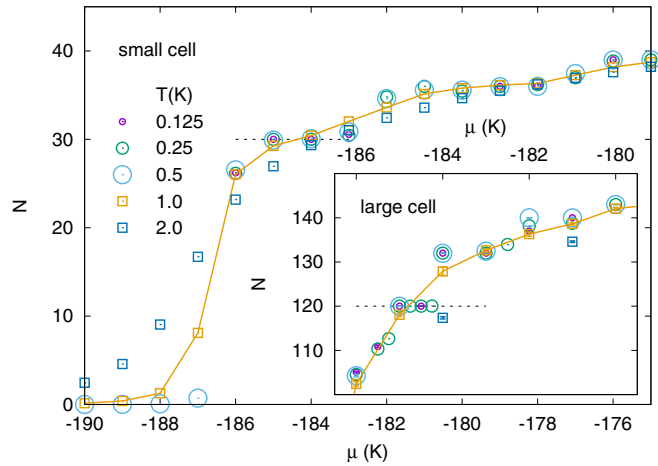
FIG. 3. ^{4}He adsorbed on GF: number of atoms as a function of the chemical potential calculated for various temperatures, as indicated, for the small cell (main figure) and the large cell (inset). The dashed lines indicate the numbers at filling 1/6.

representation of the operator $e^{-\beta H}$ mentioned above for PIMC to calculate expectation values on the quantum state $\Psi_\beta = e^{-\beta H}\Psi$, where the trial function Ψ is a closed-form approximation to the ground state. We use a trial function of the form

$$\Psi(R) = \exp\left[-\sum_i u_1(z_i) - \sum_{i<j} u_2(r_{ij})\right], \qquad (2)$$

where the one-body He-substrate pseudopotential u_1 and the two-body He-He pseudopotential u_2 are parametrized with six variational parameters each and optimized by energy minimization using the stochastic reconfiguration method [29]. For $\beta \to \infty$ the state Ψ_β approaches the exact ground state. Thus, in addition to the finite-τ bias, one has to control the error incurred using a necessarily finite value of β. We use $\beta = 2$ K^{-1}; examples of convergence in β are shown in the Appendix.

We use either "small" or "large" simulation cells, respectively containing 180 or 720 adsorption sites for GF, and half that many sites for hBN and G. For GF we will also present a few results for a larger cell with 2880 sites.

A. GF

The initial configuration for our PIMC simulations in the grand canonical ensemble is the empty cell. After equilibration, the number of ^{4}He atoms fluctuates around a stationary average value N which depends on the input chemical potential μ. Figure 3 shows a plot of $N(\mu)$ at various temperatures.

For the small cell (main figure) the data for $T = 2$ K follow a smooth curve, corresponding to a fluid phase extending over the whole range of μ shown in the plot. Upon lowering the temperature below $T = 1$ K, a flat region at $N(\mu) = 30$ develops between $\mu = -185$ and -184 K. Here the ^{4}He atoms form a commensurate solid phase with areal density $\rho = 0.0574$ Å^{-2}, at 1/6 of the adsorption sites. A fluid phase is found in a narrow region around $\mu = -186$ K, and for lower values of the chemical potential the density drops abruptly to
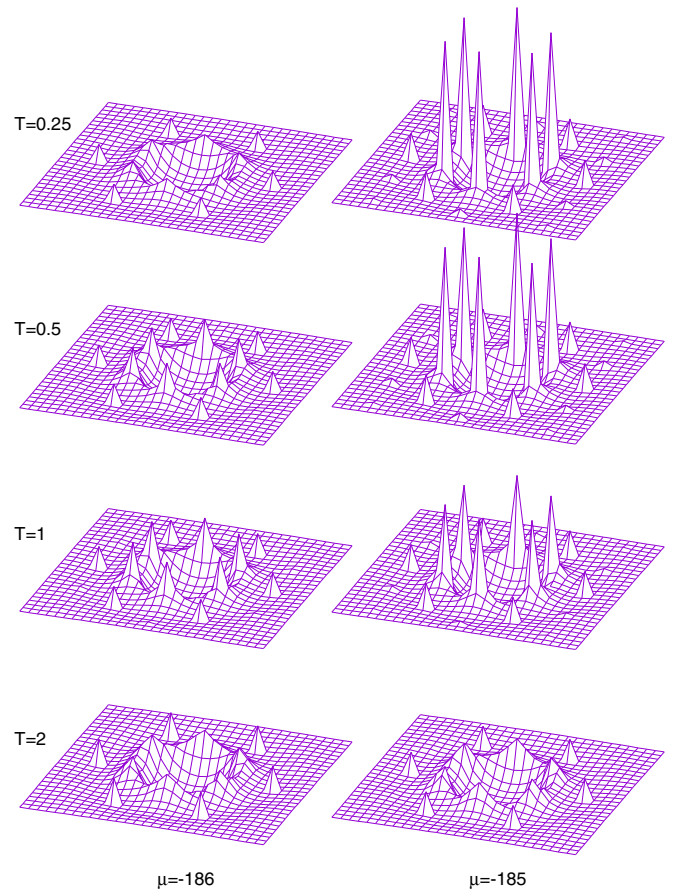

FIG. 4. ^{4}He adsorbed on GF: two-dimensional structure factor calculated in the small cell for various temperatures, as indicated in the body of the figure, at chemical potential $\mu = -186$ K (left panels) and $\mu = -185$ K (right panels). The highest peaks are 6.2 tall.

zero. At low temperature, these results depict the system as a modulated self-bound superfluid which undergoes a first-order phase transition into the 1/6 commensurate crystal upon increasing the density. A similar behavior is observed for the large cell (inset of Fig. 3), apart from details in the somewhat irregular increase of N after the flat region, with a tendency to form stripes in the small cell and domain walls in the large cell. We believe that these differences are finite size effects caused through steric constraints by the dimension and shape of the cells. We do not investigate this aspect further because our main interest here is in the modulated liquid and the commensurate crystal phases. For $T = 0.25$ K we also simulate an even larger cell with 11 520 adsorption sites. Starting from the empty cell, for $\mu = -186$ K we find the same liquid phase at areal density $\rho = 0.050$ Å^{-2} as for the other cells, but for higher chemical potential it takes too long to equilibrate a monocrystal at 1/6 covering. However, a starting crystal configuration with 1920 atoms remains stable even after very long runs for μ between -185 and -184 K.

These phase assignments are supported by structural data. Figure 4 shows the change in the structure factor $S(\mathbf{k})$ across the liquid-solid transition, both in temperature and chemical potential. The six highest peaks in each panel correspond to
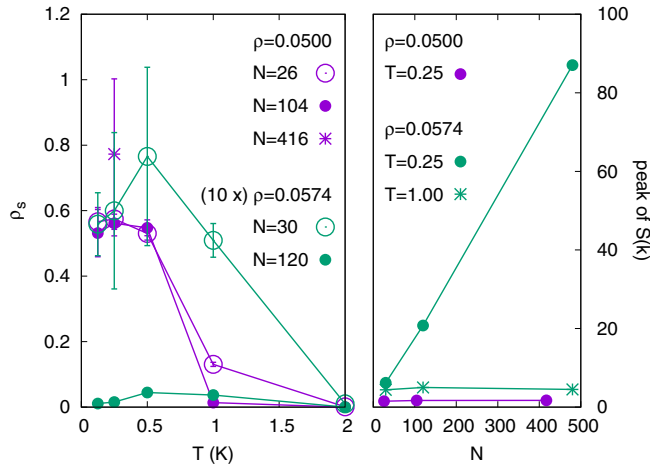
FIG. 5. ^{4}He adsorbed on GF: dependence on the system size of the superfluid fraction and of the main peak of $S(k)$ for two areal densities, $\rho \sim 0.050$ Å^{-2} (blue) and $\rho \sim 0.057$ Å^{-2} (green). Left panel: ρ_s as a function of T for various numbers N of particles; for the higher density the data are multiplied by a factor of ten. Right panel: main peak of $S(k)$ as a function of N for $T = 0.25$ and 1 K.

the first shell of reciprocal lattice vectors, $|\mathbf{k}| = 1.618$ Å^{-1}, of a triangular crystal which occupies 1/6 of the adsorption sites.

For $\mu = -186$ K, $S(\mathbf{k})$ features the characteristic ridge [7] of a strongly modulated liquid. At all temperatures six peaks are present at larger wave vectors with $|\mathbf{k}| = 2.802$ Å^{-1}; these peaks arise because the fluid has a density modulation due to the substrate adsorption potential. We note that the structure in the liquid phase is most pronounced at $T = 1$ K; for higher temperatures it is reduced by thermal fluctuations, for lower ones by Bose exchanges [10]. The liquid has a finite superfluid fraction ρ_s below a critical temperature located between $T = 0.5$ and 1 K. This is shown in Fig. 5 (left panel, blue symbols), where ρ_s is seen to exceed 50% in a wide range of system sizes for $T \leqslant 0.5$ K, while for $T = 1$ K it has a much lower value which further drops toward zero as the number of particles increases. Even at the lowest T, ρ_s is less than 100% as it is expected on general grounds for a nonuniform superfluid [30].

For $\mu = -185$ K, at low temperature the system is in the commensurate crystal phase: The main peaks of $S(\mathbf{k})$ soar to a value of 6.2 (Fig. 4), which further increases linearly with the number of particles, as shown for $T = 0.25$ K by the green circles in the right panel of Fig. 5. On the other hand for $T = 1$ the peak is still rather high (Fig. 4), but it does not increase further for larger systems (green asterisks in the right panel of Fig. 5). This indicates a melting temperature between 0.5 and 1 K. In addition to the main peaks, one notices additional weak peaks at larger k, related to the periodicity of the adsorption potential, as found in the superfluid state. The commensurate crystal is not supersolid: The small but finite superfluid fraction calculated in this phase with the small cell drops to zero as the system size increases, even at the lowest temperatures considered (green symbols in the left panel of Fig. 5).

Further details on the areal density profile $\rho(x, y)$ in the superfluid and the commensurate solid phases are given in Fig. 6. In the liquid phase (top panels) the ^{4}He atoms distribute rather uniformly along the potential valleys connecting the
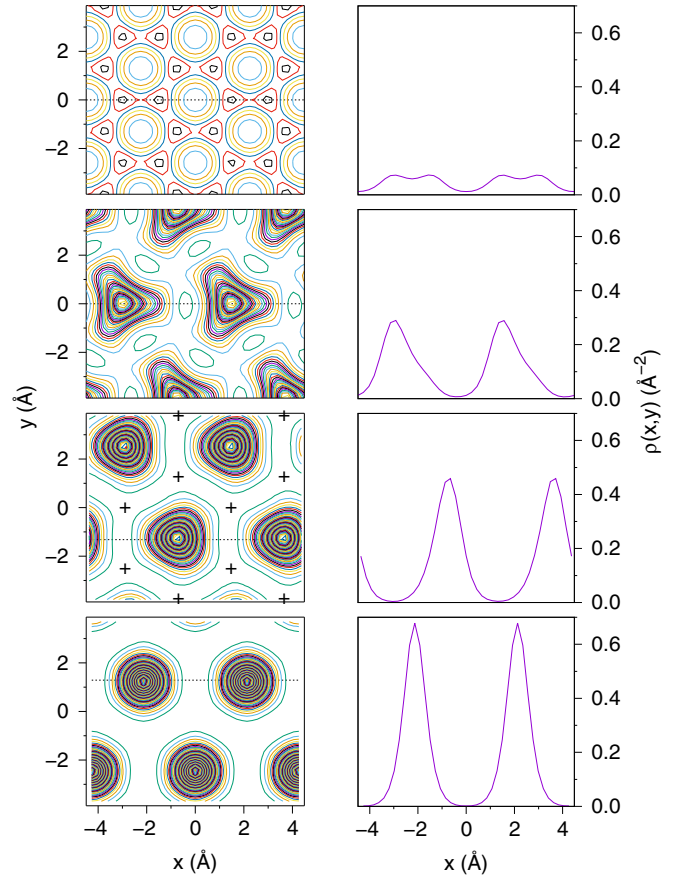

FIG. 6. One-body areal density profile $\rho(x, y)$ of ^{4}He adsorbed on various substrates at $T = 0.25$ K. Left panels: from top to bottom, superfluid at equilibrium density on GF; commensurate solid on GF; commensurate solid on hBN; commensurate solid on G in the presence of an external electric field of 1 V/Å. The contour level increment is 0.01, and the lowest level is 0.02 in the top panel and 0.01 in the other ones. For GF, the adsorption sites correspond to the maxima (black contour lines) in the top left panel; for hBN, the (unoccupied) adsorption sites are marked with plus signs in the third left panel. Right panels: $\rho(x, y)$ along the dotted line shown in the corresponding left panel.

adsorption sites. In the solid phase (second top panels) $\rho(x, y)$ features strongly anisotropic peaks centered on an adsorption site with shoulders on its three nearest neighbors and faint tails on its six second nearest neighbors. Such peaks are broader and lower than for commensurate crystal phases of ^{4}He on other substrates such as hBN or G. The local density is spatially very anisotropic; the ratio between the largest and the lowest local density is about 40.

For $T = 0$, in agreement with the low temperature results as expected, we find a transition between a modulated liquid and a commensurate solid. The energy per particle calculated for the small cell using the VPI method with a projection time $\beta = 2$ K^{-1} is shown in Fig. 7 with blue points. For $\rho < 0.0547$ Å^{-2} we can fit the Monte Carlo data with a cubic polynomial, yielding an equilibrium density $\rho_0 = 0.044 \pm 0.001$ Å^{-2}. For larger densities, the energy suddenly drops slightly below the fitted curve. In particular, for coverage 1/6, the structure factor is very similar (with minor quantitative
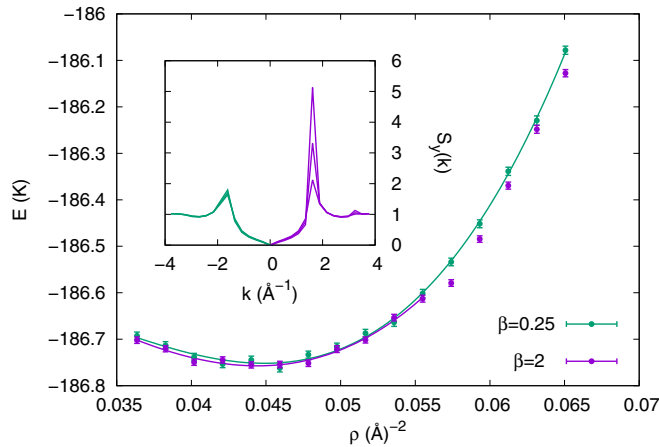
FIG. 7. ^{4}He adsorbed on GF: energy per particle as a function of the areal density ρ at $T = 0$ calculated in the small cell with projection time $\beta = 2$ K^{-1} (blue). The line is a polynomial fit, restricted to the data in the liquid phase. For areal density $\rho = 0.0574$ Å^{-2}, the system is in the commensurate solid phase, in agreement with the finite temperature calculations. The inset shows the structure factor along the y axis of reciprocal space for $\rho = 0.0536, 0.0555$, and 0.0574 Å^{-2}, in order of increasing peak height. For comparison, we include the energy and the structure factor obtained with $\beta = 0.25$ K^{-1} (green).

differences discussed in the Appendix) to that shown in the top right panel of Fig. 4, representative of the commensurate solid. The estimated coexistence region extends between 0.0535 ± 0.005 and 0.0574 Å^{-2}.

We note that a large projection time is required to converge to the solid solution starting from the trial function of Eq. (2), which represents a liquid. As shown by the green symbols and curves in Fig. 7, a value of β similar to that employed in Ref. [7] is perfectly adequate for the liquid phase but not sufficient for coverages 1/6 and higher.

B. hBN

hBN has one adsorption site per substrate unit cell, located at the hollow point H (see Figs. 1 and 2). In the xy plane, this corresponds to a minimum of the He-hBN potential, surrounded by saddle points at the TB and maxima at the TN sites. Therefore the corrugation of the absorption potential on hBN around an adsorption site differs from that on G and on graphite: The angular periodicity is 120° for hBN and not 60° as for G.

For sufficiently high temperature a monolayer of adsorbed ^{4}He forms a normal fluid phase. The density profile is directly shaped by the mentioned features of the corrugation potential: There is a peak centered on every H site and elongated towards the three nearest TB points, as shown in the inset of Fig. 8 for $T = 3$ K.

The dependence of the number of ^{4}He atoms on the chemical potential, obtained with PIMC simulations in the small cell for several temperatures, is shown in Fig. 8. For $T < 2$ K, we find that the average areal density stays constant over a wide range of μ, with a value $\rho = 0.0606$ Å^{-2}. This corresponds to a commensurate solid, with ^{4}He atoms occupying 1/3 of the
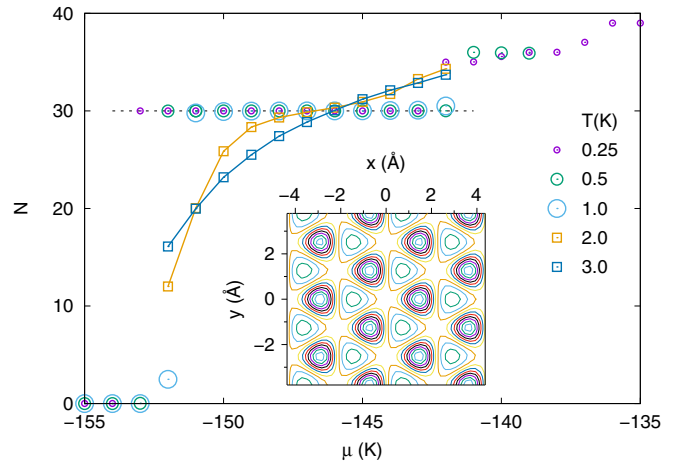

FIG. 8. ^{4}He adsorbed on hBN: number of atoms as a function of the chemical potential calculated for various temperatures, as indicated, for the small cell. We found similar results for the large cell at $T = 0.25$ K. The dashed line indicates the number of particles at $\rho = 0.0606$ Å^{-2}, corresponding to 1/3 of the adsorption sites. Inset: contour plot of the density profile in the normal fluid phase at $T = 3$ K, $\rho = 0.0606$ Å^{-2}; the contour level increment and the lowest level are both 0.01.

adsorption sites. The analysis of the structure factor across the melting temperature (which turns out to be about 2 K, Fig. 9) and its dependence on the system size (similar to that shown in Fig. 5 for GF) support this assignment.
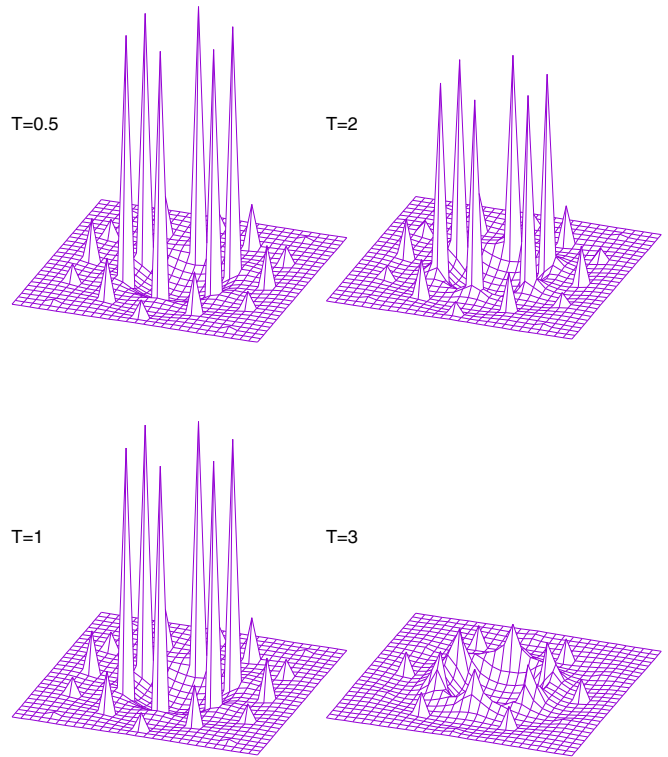

FIG. 9. ^{4}He adsorbed on hBN: two-dimensional structure factor calculated in the small cell for various temperatures, as indicated in the body of the figure, at $\rho = 0.0606$ Å^{-2} ($\mu = -146$ K, see Fig. 8). The highest peaks are 10.4 tall.
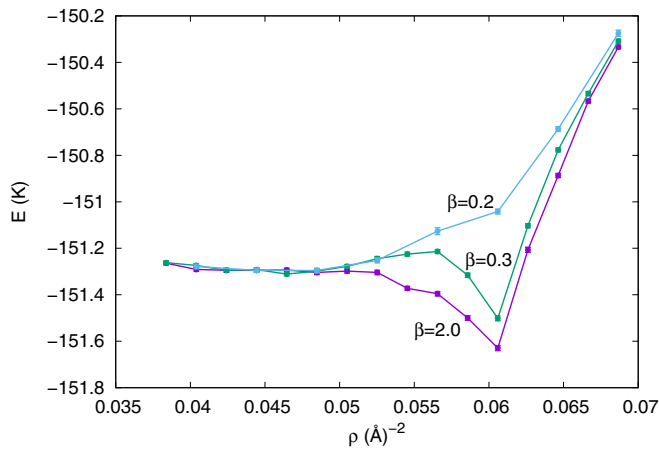
FIG. 10. ^{4}He adsorbed on hBN: energy per particle as a function of the areal density ρ calculated in the small cell with VPI simulations. In order to illustrate the convergence toward the unbiased results for projection time $\beta \to \infty$, we report energies calculated with $\beta = 0.2$, 0.3, and 2.0 K^{-1}.

From the height of the peaks of $S(\mathbf{k})$ and from the density profile, plotted in the third-row panels of Fig. 6, we see that the commensurate solid on hBN is significantly more localized than on GF. Analogously to the normal fluid phase at higher temperature, the density peaks in the solid are elongated in the direction of the three closest saddle points of the adsorption potential.

A more striking difference with the GF substrate is that, in PIMC simulations carried out at low temperature ($T < 0.5$ K), the system jumps directly from an empty cell to a commensurate crystal upon increasing the chemical potential. In particular, no (super)fluid phase should appear in the ground state of the system.

This is confirmed by VPI calculations at $T = 0$, which show that the commensurate solid is by far the lowest-energy state of the system (Fig. 10) and a fluid state is present at a lower density as a metastable state. Just like in the case of GF, we note that this VPI result, matching the findings of PIMC calculations at low temperature, requires larger projection times than used in Ref. [9].

C. Effect of an external electric field

We have performed PIMC simulations of ^{4}He at $T = 0.25$ K in the presence of an external electric field $E = 1$ V/Å on hBN and $E = 0.6$ V/Å on G, the two substrates with the larger dependence on E of the adsorption potential corrugation (see Table I).

The external field tends to delocalize the adsorbed atoms: For hBN, the range of chemical potential where ^{4}He is stuck in the commensurate solid phase shrinks by ~ 3 K; furthermore the peaks in the density profile get further elongated towards the nearest saddle points of the He-substrate potential. This can be seen by comparing the variation $\Delta\rho(x, y)$ of the density profile, shown in Fig. 11, with $\rho(x, y)$ itself (Fig. 6, third left panel): The directions of the positive (white) lobes of $\Delta\rho$ match those of the triangular stretching of the peaks.
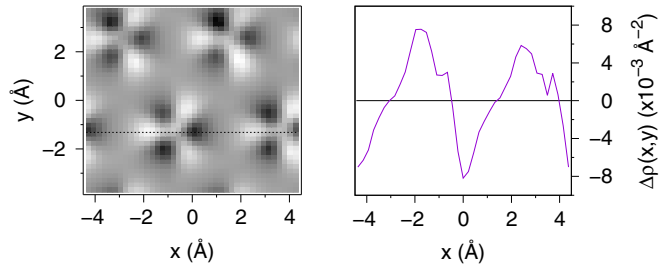

FIG. 11. ^{4}He adsorbed on hBN: variation of the density profile $\Delta\rho(x, y)$ induced by the external electric field. Left panel, grayscale map ranging from -0.08 (black) to 0.08 Å^{-2} (white); each of the pictured objects with three negative and three positive lobes is centered on a density peak of the commensurate solid (see Fig. 6, third left panel). Right panel, variation $\Delta\rho(x, y)$ along the dotted line shown in the left panel; the two structures displayed are not identical because of statistical noise (note the small scale of the plot).

However the effect is small (in fact, not visible on the scale of Fig. 6), and for both hBN and G we find that the commensurate solid remains stable, with no superfluid phases at lower densities. The density profile of the commensurate solid on G with external field is shown in Fig. 6; for a study of ^{4}He adsorbed on G without external field see Ref. [31]).

IV. SUMMARY AND CONCLUSION

In this paper we have revisited the adsorption at low coverage of ^{4}He on fluorographene and on hexagonal boron nitride in the submonolayer regime, and we have also studied such adsorption in the presence of an electric field for GF and hBN and also for graphene. The motivation was the search of a superfluid state of monolayer ^{4}He adsorbed on very regular substrates, as can be experimentally obtained with the above-mentioned substances, because such superfluid state should be characterized by a strong spatial anisotropy, a regime not yet explored with ^{4}He. For instance, in this regime rotons should be anisotropic with an energy depending on the direction of the wave vector [14] and a vortex excitation should not be translationally invariant, but it should have preferential sites for the location of the vortex core [32].

We have developed adsorption potentials for such substrates with *ab initio* methods and we have studied the properties of ^{4}He at finite temperature with PIMC and at $T = 0$ K with VPI. In the case of GF we confirm previous results [7,9] that submonolayer ^{4}He in its ground state and at low T is a low-coverage self-bound superfluid. A commensurate state is present at higher coverage in which one sixth of the adsorption sites are occupied. This commensurate state was not detected in the previous studies. In the present work we have not studied the system at higher coverage. The superfluid fraction at the lowest T is about 55% and not 100%, a depletion expected even at $T = 0$ K for a nonuniform superfluid [30]. We estimate a transition temperature to the normal state between 0.5 and 1.0 K. We have characterized the structural properties in direct and in reciprocal space confirming the extremely large spatial anisotropy of the superfluid. The superfluid fills the bonds of a honeycomb lattice of the adsorption sites with a ratio of about 6 between the largest and

the smallest areal density: it is like the superfluid was moving in a multiconnected space. The commensurate state at coverage 1/6 of the adsorption sites is a triangular lattice similar to the commensurate state of ^{4}He on graphite at coverage 1/3 but special features characterize the commensurate state on GF. In fact, even at the lowest T a ^{4}He atom is not constrained to remain at a single adsorption site but there is a sizable probability of occupation of the neighboring sites giving rise to a three-lobed density distribution. It will be of interest to determine if such behavior, to our knowledge unique among the ordered adsorbates on regular substrates, is modifying the order-disorder phase transition compared to that of ^{4}He on graphite [8]. Other features of this ordered state of ^{4}He on GF are a mean square deviation from the equilibrium site more than double that of ^{4}He on graphite and a particularly low transition temperature to a disordered state between 0.5 and 1 K, less than one third of the order-disorder transition of ^{4}He on graphite. This commensurate state is not supersolid.

We find that the lowest energy state of ^{4}He on hBN at $T = 0$ K and at low T is a commensurate triangular solid in which one third of the adsorption sites are occupied, a state isomorphous to that of ^{4}He on graphite and graphene. The temperature of the order-disorder transition is about 2 K. The present result modifies the conclusion of a previous study [9] in which it was found that the ground state was a superfluid. We have verified that this discrepancy is due to the use of a too short projection time in the earlier $T = 0$ K study. At coverage below this commensurate state a fluid state is present as a metastable one. We have shown that an electric field up to 1.0 V/Å tends to delocalize the adsorbed atoms, but the effect is small and the electric field does not modify the phase behavior of the system. We find that also in the case of G the ground state of submonolayer ^{4}He remains an ordered state commensurate with the adsorption sites at coverage 1/3.

In conclusion, on present theoretical evidence the only regular substrate that supports a superfluid ground state is GF. Possibly this is also true for graphane [7], a compound isomorphous to GF with the fluorine atoms replaced by the hydrogen ones, but experimentally it is difficult to produce regular substrate with full stoichiometry, and we have not investigated this system with *ab initio* methods. The different nature of the lowest energy state of ^{4}He on GF compared to that on hBN, G, and graphite is mainly due to the number of adsorption sites per surface unit cell, twice as many for GF as for the other substrates. As seen in Fig. 12 this entails a larger, interconnected region of favorable, low potential energy available to the helium atoms. The size and shape of such a region stabilize the superfluid phase and induce the three-lobed distortion of the peaks in the commensurate solid.

Other commensurate states might be present at larger coverage between the density range of the present study and the promotion coverage to the second layer; this is an interesting topic for future studies. Another interesting development is the study of the adsorption of the fermionic ^{3}He on GF and on hBN. Due to the smaller mass of ^{3}He it is very unlikely that the ground state of ^{3}He on GF is a commensurate ordered state so that the low coverage state should be a liquid or an unbounded gas. Some evidence for a liquid state was found in the earlier study [7] with the semiempirical adsorption pot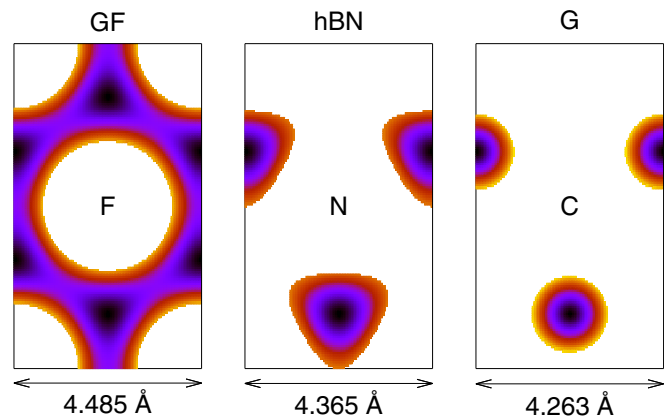ential so further study of the fermionic system with the *ab initio* adsorption potential is of great interest because, in any case, ^{3}He on GF opens the possibility of studying a strongly interacting Fermi system with large spatial inhomogeneity. We have shown that the most stable state of ^{4}He on hBN is ordered and a fluid state is only a metastable one. The smaller mass of ^{3}He might alter the balance between these two states. In fact, we have performed PIMC computations for bosonic $m = 3$ and indeed we find that with this mass the fluid state is the stable one. Of course, the Fermi statistics might alter this result, and this is left for future study. On this issue it will be important to perform new experiments on ^{3}He on hBN to verify the earlier measurements [33] that gave some evidence for a localized commensurate state.

FIG. 12. The x, y classically allowed regions for a ^{4}He atom on GF, hBN, and G at a distance d from the substrate corresponding to the minimum value $V_{\min}$ of the adsorption potential. The color maps represent the adsorption potential $V(x, y) - V_{\min}$ from zero to the kinetic energy of a single ^{4}He atom on the substrate calculated with PIMC at $T = 0.25$ K (i.e., 27.0, 22.6, and 28.4 K for GF, hBN, and G, respectively). The color scale ranges from 0 (black) to 28.4 K (yellow). The plots are centered on the less favored site (F atom for GF, N atom for hBN, and C atom for G). In the superfluid phase of ^{4}He on GF (top panels of Fig. 6), the adsorbate atoms cover rather uniformly the interconnected regions of low potential energy.

APPENDIX

The PIMC simulations [10,28] give unbiased thermal averages for $\tau \to 0$. We use the primitive action with $\tau = 0.002$ K^{-1} which entails a negligible error in the quantities of main interest here, namely the superfluid fraction ρ_s, calculated using the so-called winding number estimator, [10] and the static structure factor $S(\mathbf{k})$, calculated as the average of
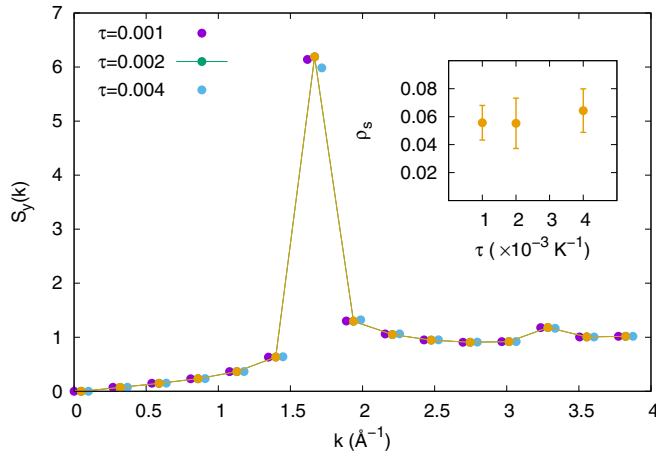
FIG. 13. The structure factor along the *y* axis of reciprocal space for $N = 30$ ^{4}He atoms adsorbed on GF in the 1/6 commensurate solid phase, calculated with PIMC at $T = 0.25$ K. Data for different values of τ are slightly offset in *k* for clarity. The inset shows the superfluid fraction as a function of τ.
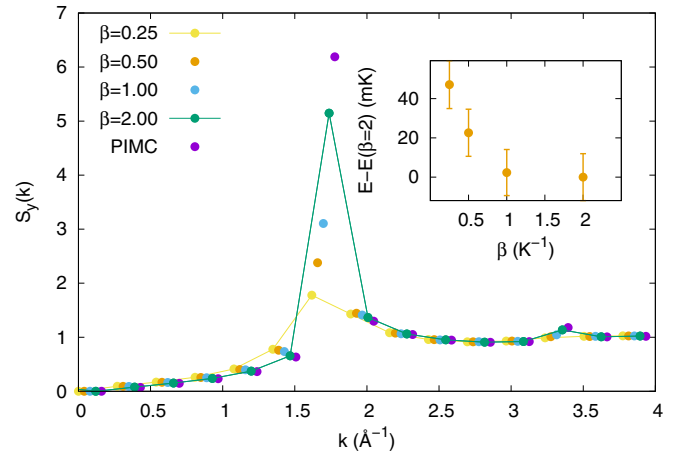

FIG. 14. The structure factor along the *y* axis of reciprocal space for $N = 30$ ^{4}He atoms adsorbed on GF at the density of the 1/6 commensurate phase, calculated with VPI. Data for different values of β are slightly offset in *k* for clarity. The PIMC result for $T = 0.25$ K is also shown for comparison. The inset shows the energy per particle as a function of β, relative to its value at $\beta = 2$ K^{-1}.

$\sum_{ij} \exp[-i\mathbf{k} \cdot (\mathbf{r}_i - \mathbf{r}_j)]/N$ over the sampled configurations. This is shown in Fig. 13 for $N = 30$ ^{4}He atoms adsorbed on GF in the 1/6 commensurate solid phase (here the nonzero value of the superfluid fraction is a finite-size effect).

The VPI simulations [10,11] give unbiased ground state results for time step $\tau \to 0$ and projection time $\beta \to \infty$. We use the primitive action with the same value $\tau = 0.002$ K^{-1} as in PIMC, and $\beta = 2$ K^{-1}. The convergence in β is shown in Fig. 14 for the structure factor and the energy. In the range of β between 0.25 and 2 the energy changes merely by

$\sim$50 mK, but the structure factor develops large peaks at the first reciprocal lattice vector of the commensurate solid. The convergence in β of the main peaks is not complete, because their height should be closer to that obtained with PIMC at the lowest temperatures (also shown in Fig. 14 for comparison). Nevertheless, a projection time of $\beta = 2$ K is clearly sufficient to turn the liquid state represented by the trial function of Eq. (2) into a solid.

[1] M. Greiner, O. Mandel, T. Esslinger, T. W. Hansch, and I. Bloch, Nature (London) **415**, 39 (2002).

[2] L. W. Brunch, M. W. Cole, and E. Zaremba, *Physical Adsorption: Forces and Phenomena* (Dover Publishing, Mineola, NY, 2007), Section 6.1.

[3] M. E. Pierce and E. Manousakis, Phys. Rev. Lett. **83**, 5314 (1999).

[4] P. Corboz, M. Boninsegni, L. Pollet, and M. Troyer, Phys. Rev. B **78**, 245414 (2008).

[5] P. A. Crowell and J. D. Reppy, Phys. Rev. B **53**, 2701 (1996).

[6] J. Nyeki, A. Phillis, A. Ho, D. Lee, P. Coleman, J. Parpia, B. Cowan, and J. Saunders, Nat. Phys. **13**, 455 (2017).

[7] M. Nava, D. E. Galli, M. W. Cole, and L. Reatto, Phys. Rev. B **86**, 174509 (2012).

[8] L. Reatto, D. E. Galli, M. Nava, and M. W. Cole, J. Phys.: Condens. Matter **25**, 443001 (2013).

[9] P. L. Silvestrelli, M. Nava, F. Ancilotto, and L. Reatto, J. Low Temp. Phys. **196**, 42 (2019).

[10] D. M. Ceperley, Rev. Mod. Phys. **67**, 279 (1995).

[11] A. Sarsa, K. E. Schmidt, and W. R. Magro, J. Chem. Phys. **113**, 1366 (2000).

[12] M. Rossi, M. Nava, L. Reatto, and D. E. Galli, J. Chem. Phys. **131**, 154108 (2009).

[13] L. Reatto, M. Nava, D. E. Galli, C. Billman, J. O. Sofo, and M. W. Cole, J. Phys.: Conf. Ser. **400**, 012010 (2012).

[14] M. Nava, D. E. Galli, M. W. Cole, and L. Reatto, J. Low Temp. Phys. **171**, 699 (2013).

[15] M. J. Stott and E. Zaremba, Phys. Rev. B **22**, 1564 (1980); G. Vidali, M. W. Cole, and C. Schwartz, Surf. Sci. **87**, L273 (1979); K. T. Tang and J. P. Toennies, J. Chem. Phys. **80**, 3726 (1984).

[16] P. Giannozzi, S. Baroni, N. Bonini, M. Calandra, R. Car, C. Cavazzoni, D. Ceresoli, G. L. Chiarotti, M. Cococcioni, I. Dabo, A. Dal Corso, S. De Gironcoli, S. Fabris, G. Fratesi, R. Gebauer, U. Gerstmann, C. Gougoussis, A. Kokalj, M. Lazzeri, L. Martin–Samos, N. Marzari *et al.*, J. Phys.: Condens. Matter **21**, 395502 (2009).

[17] R. Sabatini, T. Gorni, and S. de Gironcoli, Phys. Rev. B **87**, 041108(R) (2013).

[18] O. A. Vydrov and T. Van Voorhis, J. Chem. Phys. **133**, 244103 (2010).

[19] P. L. Silvestrelli and A. Ambrosetti, Phys. Rev. B **91**, 195405 (2015).

[20] P. L. Silvestrelli and A. Ambrosetti, J. Low. Temp. Phys. **185**, 183 (2016).

[21] J. Neugebauer and M. Scheffler, Surf. Sci. **287–288**, 572 (1993).

[22] L. Bengtsson, Phys. Rev. B **59**, 12301 (1999).

[23] B. Meyer and D. Vanderbilt, Phys. Rev. B **63**, 205426 (2001).

[24] J. H. J. Ostrowski and J. D. Eaves, J. Phys. Chem. B **118**, 530 (2014).

[25] Three dimensional tabulations of the He-substrate potentials are available upon request from one of the authors (F.A.).

[26] In particular, minor numerical differences in the adsorption potential with respect to the data reported in Ref. [9] using the same functional are due to slightly better convergence in energy and in the optimization of the equilibrium structure, and in the use of a wider vacuum region separating the periodically repeated slabs.

[27] R. A. Aziz, V. P. S. Nain, J. S. Carley, W. L. Taylor, and G. T. Conville, J. Chem. Phys. **70**, 4330 (1979).

[28] M. Boninsegni, N. V. Prokof'ev, and B. V. Svistunov, Phys. Rev. E **74**, 036701 (2006).

[29] S. Sorella, M. Casula, and D. Rocca, J. Chem. Phys. **127**, 014105 (2007).

[30] A. J. Leggett, J. Stat. Phys. **93**, 927 (1998).

[31] Y. K. Kwon and D. M. Ceperley, Phys. Rev. B **85**, 224501 (2012).

[32] A. Gallemi, S. M. Roccuzzo, S. Stringari, and A. Recati, Phys. Rev. A **102**, 023322 (2020); F. Ancilotto, M. Barranco, M. Pi, and L. Reatto, *ibid.* **103**, 033314 (2021).

[33] T. P. Crane and B. P. Cowan, Phys. Rev. B **62**, 11359 (2000); Y. Tang and N. S. Sullivan, J. Phys.: Conf. Ser. **568**, 012018 (2014).